A new microfluidic device design for a defined positioning of neurons *in vitro*

Katharina Walczuch,[1,a),b)] Peter Renze,[2,b)] Claudia Ingensiep,[1] Rudolf Degen,[1] Thanh Phong Bui,[1] Uwe Schnakenberg,[3] Peter Bräunig,[1] and Katrin Bui-Göbbels[1]

[1]*Institute of Biology II, RWTH Aachen University, Worringerweg 3, 52074 Aachen, Germany*
[2]*Institute of Energy and Drive Technologies, Hochschule Ulm, Eberhard-Finckh-Str. 11, 89075 Ulm, Germany*
[3]*Institute of Materials in Electrical Engineering 1, RWTH Aachen University, Sommerfeldstraße 24, 52074 Aachen, Germany*

(Received 27 April 2017; accepted 29 June 2017; published online 12 July 2017)

A new triangle-shaped microfluidic channel system for defined cell trapping is presented. Different variants of the same basic geometry were produced to reveal the best fitting parameter combinations regarding efficiency and sensitivity. Variants with differences in the trap gap width and the inter-trap distance were analyzed in detail by Computational Fluid Dynamics simulations and in experiments with artificial beads of different sizes (30, 60, 80 μm). Simulation analysis of flow dynamics and pressure profiles revealed strongly reduced pressure conditions and balanced flow rates inside the microfluidic channels compared to commonly used systems with meandering channels. Quantitative experiments with beads showed very good trapping results in all channel types with slight variations due to geometrical differences. Highest efficiency in terms of fast trap filling and low particle loss was shown with channel types having a larger trap gap width (20 μm) and/or a larger inter-trap distance (400 μm). Here, experimental success was achieved in almost 85% to 100% of all cases. Particle loss appeared significantly more often with large beads than with small beads. A significantly reduced trapping efficiency of about 50% was determined by using narrow trap gaps and a small inter-trap distance in combination with large 80 μm beads. The combination of the same parameters with small and medium beads led to an only slight decrease in trapping efficiency (80%). All channel types were tested qualitatively with invertebrate neurons from the pond snail *Lymnaea stagnalis*. The systems were appropriate to trap those sensitive neurons and to keep their viability in the trapping area at the same time. *Published by AIP Publishing.* [http://dx.doi.org/10.1063/1.4993556]

I. INTRODUCTION

The investigation of basic developmental processes within neuronal networks, such as path-finding and plasticity, requires observation over a longer period of time.[1] To gain detailed insight in network activity, monitoring individual network participants and their influence on the overall network dynamics is necessary. For this purpose, the use of *in vitro* approaches can be advantageous compared to investigations *in vivo* as the reduced number of network participant allows for an unambiguous assignment of signals to certain cells.[2,3] In this context, the use of non-invasive recording techniques, measuring the cell activity extracellularly, is state of the art and multielectrode arrays (MEAs) are most effective tools.[4–7] Generally, MEA chips are equipped with culture chambers. Because cells applied to such chambers distribute randomly

[a)]Author to whom correspondence should be addressed: walczuch@bio2.rwth-aachen.de
[b)]K. Walczuch and P. Renze contributed equally to this work.

over the MEA surface, it becomes necessary to strongly increase the cell density for covering all electrodes. Complementary metal oxide semiconductor (CMOS) technology, for example, allows the use of high density MEAs with up to thousands of electrodes.[8,9] However, with such high densities still only a fraction of cells can be monitored simultaneously and never the entire network. Therefore, also in *in vitro* approaches, the number of network participants has to be lowered extremely; otherwise, an unambiguous assignment of certain signals to individual cells remains a problem.[9] To achieve a maximum of spatial resolution, it is desirable to culture precisely one neuron per electrode, and ideally, the neuron should cover the electrode completely to achieve optimal recording conditions.[10] Therefore, cells should be of adequate size as electrodes of standard MEAs generally are not smaller than about 30 μm. The achievement of a combination of good signal-to-noise ratios, low-density culture, and directed positioning of cells on the electrodes is still the prominent challenge in this field of research. In this context, the use of invertebrate neurons provides several advantages because in contrast to vertebrate cells they can be cultured at extremely low density.[2,3,11] Furthermore, many neurons from invertebrates, like snails and locusts, are very large (up to 100 μm and more). That way, they can be manipulated individually and they are able to cover individual electrodes completely. However, the defined positioning of cells *in vitro* is still a critical point. Besides the possibility to pattern the surface with adhesive chemicals for defined cell positioning and growth,[12] manual positioning on predefined locations in topographically raised microstructures showed promising results.[13–17] Such solutions, however, have deficits as well. They lack efficiency, spatial and temporal control over the extracellular microenvironment, and the cells may be subjected to stress by the manual manipulation during positioning. Microfluidic devices consisting of closed channels and chambers with growth guiding structures but with more or less static bath conditions were shown to be useful solutions regarding increased control, for example, in co-culture application.[18,19] The ability to apply continuous fluidic flow inside the channels further increases the level of control over the cellular environment.[20–22]

Until now, the hydrodynamics of a continuous flow was used only rarely to guide individual cells from a low density cell suspension to defined positions within a closed microfluidic system.[23–27] The most successful approaches yielding good single cell trapping results used the concept of different fluidic resistances in different channel geometries by using a serpentine or square waved geometry for a main channel and much smaller and shorter transverse channels of less fluidic resistance for cell and particle trapping.[24,25,27–30] This concept showed successful results with artificial particles[28] and high density cell suspensions of different types of cells, like yeast cells,[27] different kinds of cancer cells,[24] or different kinds of stem cells[25,29] for example. In rare cases, mammalian neurons were applied to such microfluidic systems as well.[30] However, to the best of our knowledge, despite their advantages in terms of basic network research and the ongoing positioning and growth guiding problem of cells on MEA surfaces, positioning neurons from invertebrates by fluidic flow in closed microfluidic channels has not yet been reported.

As a precursor to neuronal network studies using MEAs, the cell positioning problem has to be tackled first. Therefore, we focused on the development of a new and suitable channel geometry for positioning of neurons and sensitive cells generally at defined locations. In the course of this study, invertebrate neurons were used to analyze the suitability of systems with meandering main channels as commonly used. Although various different designs were tested, the desired trapping results could not be achieved. Also the viability of both pond snail and locust neurons suffered strikingly (data not shown). To meet the requirements of our test object of choice, namely neurons from the pond snail *Lymnaea stagnalis*, and to improve geometrical disadvantages of common designs, a new triangle shaped closed microfluidic channel design for single and low density cell trapping at defined positions was developed.

The new channel geometry thereby possesses essential advantages in the context of a lowered pressure profile, which corresponds to a decreased mechanical stress for the cells. As a result, for the first time, defined positioning of sensitive invertebrate neurons could be managed hydrodynamically within a closed microfluidic channel system by a continuous flow.

II. MATERIALS AND METHODS

A. General conceptual design

Microfluidic devices for cell trapping were always composed of a main channel, connecting an inlet and an outlet and a transverse channel system. The transverse channels contained a "trap gap" area where the channel narrows to dimensions smaller than the particles to be captured. The area directly upstream from the trap gap represented the cell trap. Generally, the number of transverse channels always corresponded to the number of cell traps.

In such a microfluidic system, streamlines can be observed, which are on the one hand directed into the transverse trap channels and on the other hand follow the main channel direction. Therefore, a certain part of particles would be directed towards the transverse channels ending in a trap. Once a cell occupies a trap, it is thought to act as a plug, leading to an immediate increase of the flow resistance in this particular transverse channel. The main flow is redirected to the main channel and to the downstream transverse channels, respectively. The new geometric design based on this basic assumption is shown in Fig. 1. The main channel of the new system consisted of two channel flanks arranged at right angle connecting inlet and outlet. Oblique transverse channels interconnect these two flanks forming the hypotenuse of a triangle. The transverse channels formed short cuts between the main channel flanks. Each transverse channel contained a single cell trapping area where the width of the oblique channel is reduced to a size much less than the average soma diameter for a short distance. The oblique transverse channels originated at different locations of the main channel, each forming a triangle with different side lengths. Funnel shaped stretches connected the main channels to inlet and outlet. These regions facilitated inward and outward transfer of the cells. Different

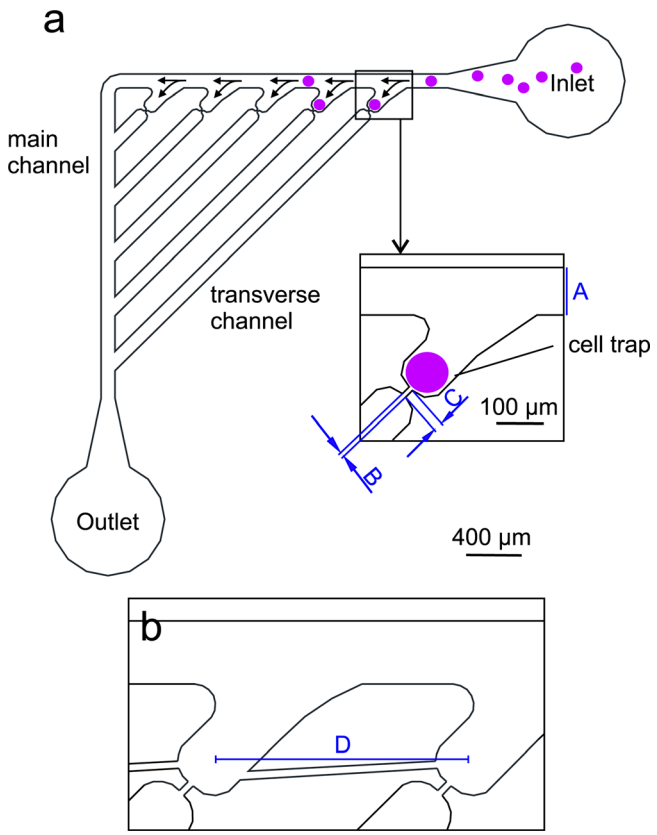

FIG. 1. (a) Design of a microfluidic channel system for cell trapping. Arrows indicate direction of fluid flow. Trapping area shown in detail (inset) to illustrate the geometrical parameters: A: 100 μm; B: 10 μm; C: 20 μm; channel height (not shown in schematic) is 100 μm. (b) A variant of trapping areas with interconnecting channels for neurite outgrowth. D: Inter-trap distance measured from trap center to trap center.

prototypes with variations of certain parameters were designed to test best trapping conditions but also to match potential MEA-electrode arrangements.

An overview of the parameter combinations leading to 10 prototypes is provided in Table I. As shown in Fig. 1, the main parameters were the main and transverse channel width and height (A), the narrow part of the transverse channel part downstream the trapping area, the trap gap (B), the length of the trap gap (C), and the distance between the trapping areas (D). As large neurons can be up to 100 μm, channels must be at least 100 μm in width and height to avoid channel clogging. In this study, the channel width and height (A) were constant throughout the different subtypes having 100 μm each. Furthermore, the length of the trap gap (C) was also constant and equals 20 μm. Two different trap gap widths (B), 10 and 20 μm, were tested. Furthermore, two different inter-trap distances (D), of either 200 μm or 400 μm, corresponding to inter-electrode distances of two different commercially available MEA types (measured from center to center) were tested. Moreover, prototypes with either 5 or 9 traps were produced. Based on the parameters of channel types 3 and 5 (see Table I), the subtypes 9 and 10 additionally provide small channels allowing for neurite growth and possible network formation of neighboring neurons. These so-called neurite channels had a height of 5 μm and a width of 10 μm.

It is not expected that the global flow parameters are changed by a varying trap number or the presence of neurite channels. Therefore, only prototypes with 5 traps, different trap gap widths and varying inter-trap distance (channel types 1, 2, 5, and 6; see Table I), were analyzed in detail by simulation and quantitative experiments with beads. However, snail neuron experiments were performed for all prototypes to generate qualitative results.

B. Simulation

In the present work, the laminar and incompressible flow field in a microfluidic environment has been analyzed by numerical simulations using the open-source software OpenFOAM®.[31–33]

In particular, the solver *simpleFOAM* was applied to solve the three-dimensional Navier-Stokes equations. For the spatial discretization, the following schemes have been chosen: limited central differences with 2nd order accuracy for gradient, upwind differencing with 2nd order accuracy for divergence, and a limited non-orthogonal correction algorithm for the Laplacian terms.[32]

The computational mesh was generated using *snappyHexMesh*, which is part of the OpenFOAM library. Approximately 16 cells of uniform size are distributed over the channel width (100 μm) with further stepwise refinement near the cell traps. On the solid surfaces, up to three prism cell layers are inserted to further improve the near wall resolution. The maximum number of cells is approximately 1 million for the triangle shape configurations and between 1.8 and 2.2 $\times$ 10^6 cells for the serpentine shapes.

TABLE I. Parameter variations of 10 microfluidic channel types.

Channel type	Trap gap width (B) (μm)	Trap distance (D) (μm)	Trap number	Neurite channel
1	10	200	5	–
2	20	200	5	–
3	10	200	9	–
4	20	200	9	–
5	10	400	5	–
6	20	400	5	–
7	10	400	9	–
8	20	400	9	–
9	10	400	5	+
10	10	200	9	+

Three basic boundary conditions were applied for all simulations: a standard no-slip wall boundary condition, fixed velocity as well as pressure extrapolation at the inlet, and fixed pressure as well as velocity extrapolation at the outlet boundary. The material properties are those of liquid water, and the volumetric flow rate has been set according to the experiments as $\dot{V} = 1\,\mu\text{l/min}$.

C. Template production

For mask production, the channel geometries were drawn with AutoCAD (Autodesk Inc., San Rafael, California). Afterwards, the SU-8-based templates were fabricated on silicon wafers with photolithographic techniques. Details were described previously.[17]

D. Device production

Final channel structures were prepared from polydimethylsiloxane (PDMS; Sylgard 184, Dow Corning Co., Midland, Michigan) molds from the corresponding templates. To obtain channel structures, liquid PDMS was mixed with the curing agent at 10:1 and pored over the wafer. PDMS was cured within 45 min at 60 °C. The hardened replica was peeled off the wafer, and single channel structures were cut from the silicone layer. Afterwards, channel inlets and outlets of 0.8 mm diameter were punched out under microscopic control. The devices were bonded on glass slides via oxygen plasma.

E. Experimental setup

Silicon tubes (Microtube PTFE, Adtech Polymer Engineering Ltd, Stroud, UK) of 0.3 mm inner diameter, 0.76 mm outer diameter, and approximately 30 cm in length were inserted to the inlet and outlet of the channel system, which was positioned on the stage of an inverse microscope (Olympus CKX41, Olympus Europe GmbH, Hamburg). The other end of the inlet tube was connected via Luer lock (Globaco GmbH, Rödermark, Germany) to a 5 ml plastic syringe filled with 70% ethanol. Handling of the syringe was managed manually or by a syringe pump (LA-100, Landgraf Laborsysteme HLL GmbH, Langenhagen, Germany). The other end of the outlet tube was placed into a waste vessel. The channel system was perfused with ethanol for sterilization at a velocity of $50\,\mu\text{l}\cdot\text{min}^{-1}$ driven by the syringe pump or by manual pressure. Good care was taken on the removal of all air bubbles in the channel system. Subsequently, the syringe was replaced by a second syringe of the same type filled with sterile phosphate buffered saline (PBS), and the system was perfused a couple of minutes to remove the ethanol. Cell loading procedure is schematically presented in Fig. 2: a 100 μl low binding pipette tip was filled with a culture medium. While the perfusion flow with PBS was still running, the inlet tube end which has been stuck in the inlet of the channel system was replaced by the pipette tip filled with medium. For experiments with polystyrene beads, distilled water was used

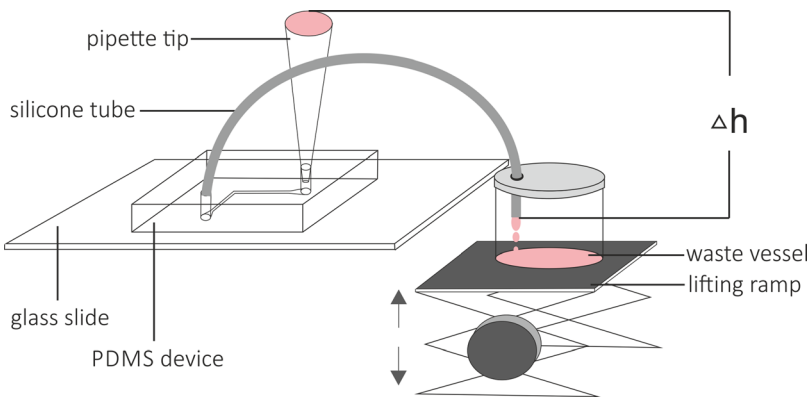

FIG. 2. Schematic drawing of the experimental setup at the step of cell loading (not true to scale).

instead of ethanol and culture medium. The waste vessel was positioned on a small lifting platform, on a level 30 cm below the level of the channel system. This difference in height (Δh: see Fig. 2) resulted in the continuous medium flow by gravity feed at about 30 μl/min and flow velocity could be adjusted by lifting or lowering the platform. As the medium in the inlet tip slowly drained off during perfusion, it was refilled as required. Just before cell/bead loading, the velocity of the medium flow was strongly lowered to 1 μl/min by lifting the platform accordingly.

F. Beads

For experiments with particles, polystyrene beads (Micromod Partikeltechnologie GmbH, Rostock, Germany) of different diameters (30, 60, and 80 μm) were applied. A volume of 30 μl bead suspension (1 bead/μl distilled water) was introduced into the inlet. Flow behavior of beads was observed through the inverse microscope, and trapping success was documented by photos and videos for subsequent offline analysis using a microscope camera (Moticam 3.0 MP, Motic GmbH, Wetzlar, Germany).

To quantitatively evaluate the functionality and efficiency of the microfluidic channel systems, channel types 1, 2, 5, and 6 were tested with different bead sizes. Three different criteria were taken into account to evaluate the efficiency of a certain channel type for a certain particle size: 1. The general trapping success: An experiment was evaluated as successful, if all cell traps became occupied during a period of 4 min beginning with the first bead arriving at the channel system. 2. The extent of particle loss: The ratio of beads successfully directed towards the cell traps and those which were not deflected and left the system via the outlet. 3. The occurrence and extent of multitrapping: Trapping of more than one particle per trap. An experiment and therefore the time measurement started with the first particle arriving at the inlet and was finished after all traps were occupied. After this point, fluid flow was immediately stopped and no further arriving beads were included into the count. Values were compared for different designs and under consideration of different bead sizes. Experiments for this quantitative characterization were repeated at least 17 times for each tested channel type and each bead size.

G. Animals

For the study young adult pond snails of the genus *Lymnaea* from the department's own laboratory breeding stock were used. The animals were fed vegetables like cucumber and lettuce *ad libitum*. They were kept in 10 l tanks filled with tap water supplemented with an aquarium water conditioner (AquaSafe, Tetra GmbH, Melle, Germany) at room temperature and under a natural light/dark cycle. The tanks were equipped with fine sand and gravel and were ventilated by an air stone. During the winter months, the light cycle was supported by an artificial light source with a light/dark cycle of 12/12 h. For experiments, neurons from the ganglionic ring of young adults with shell lengths of 2 to 3 cm were used.[34]

The preparation of snail neurons up to the step after enzymatic treatment essentially corresponded to techniques described previously[35,36] with a few exceptions described elsewhere.[17] Four ganglia were used for neuron extraction, the two pedals, the right parietal, and the left visceral ganglia.

These ganglia possess a great number of cells on the one hand, and they contain the most cells with large soma diameters above 50 μm on the other. The neurons were mechanically dissociated using fine forceps. Close attention was paid to remove as much non-cellular tissue as possible. Thereby, selection of neurons was not limited to specific types. Generally, a small volume of 30 μl with approximately 30 to 50 neurons was introduced by a low binding pipette to the inlet of the channel system. Flow behavior of cells was observed through the inverse microscope and trapping success was documented by photos and videos for subsequent offline analysis using a microscope camera (Moticam 3.0 MP, Motic GmbH, Wetzlar, Germany). The viability of the cells at the end of an experiment was checked qualitatively. A cell was evaluated to be alive and healthy by color and shape. Viable neurons possess a bright yellow color with a slight darker center and are surrounded by a small halo. Their surface should be smooth and

defined, eventually equipped with an axon stump. Figure 3 illustrates the differences between a viable and a nonviable neuron.

III. RESULTS

A. Numerical simulation of steady stay flow field

The flow field properties for several channel types (1, 2, 5, and 6) have been analyzed by numerical simulations. The results for channel types 1 and 6, differing in trap gap width and inter-trap distance, are briefly summarized in Fig. 4. Results for channel types 2 and 5, with an opposed parameter combination compared to subtypes 1 and 6, concerning inter-trap distance and trap gap width, can be seen in the supplementary material (Fig. 1). They showed a very similar profile to that of types 1 and 6, while the trap gap width revealed to have the largest impact on the flow ratio and pressure conditions in the traps. The exact values for mass flow rate proportions in the different traps and the main path as well as for the driving pressure difference can be found in Table II.

Absolute numbers for the mass flow rates can be taken from the supplementary material (Table I). The contours of the velocity magnitude show a similar flow behavior for all trap types. In the inlet and outlet sections, the velocity magnitude is small due to the relatively large cross sectional area of the channel. The highest velocity magnitude is reached when the inlet cross section is reduced to the final channel size before the first flow split, and can be also found after the last channels have merged [Figs. 4(a) and 4(b); upper pictures]. The pressure field [Figs. 4(a) and 4(b); lower pictures] shows the expected behavior, i.e., the total static pressure is decreasing linearly with the path length from the inlet to the outlet due to wall friction. Reaching the trapping area, the flow is split into the staggered array of trapping channels. The flow velocity in the main channel is therefore further reduced after each new flow junction and is increased again in the second part of the main channel, where the flow gets merged. Although the pressure field shows a strong flow resistance at each trap, the distribution of the flow into the trapping channels is not uniform. For example, at channel type 1, this distribution ranged from about 10% in the first trap to about 4% in the last trap, while about 60% of the flow is not directed into the trap channels (Table II). This non-uniformity may assume a serial order occupancy of the traps by introduced beads or cells. The velocity magnitude at each trap type was strongly influenced by the trap gap width (Fig. 4, Table II). Narrowing the gap width naturally increased the resistance in the respective channels. While in devices with wider trap gaps (20 μm) more than 70% of the fluid volume split up on the transverse channels, this value decreased to about the half of this value by reducing the trap gap width to 10 μm. Channel

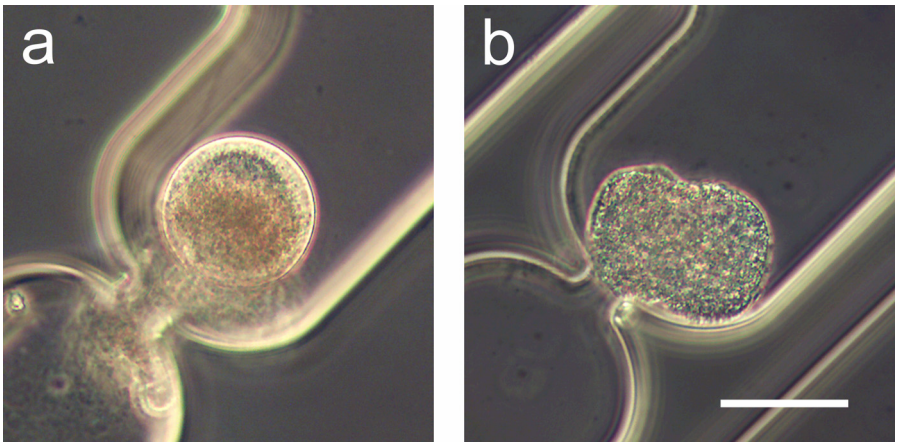

FIG. 3. Phase contrast images of trapped neurons from *Lymnaea stagnalis* in different health conditions. (a) Example for a viable neuron assessed by shape and color. (b) Example for a nonviable neuron. Note the amorphous shape, dark color, and numerous vesicular structures in the cytoplasm. Scale bar: 50 μm.

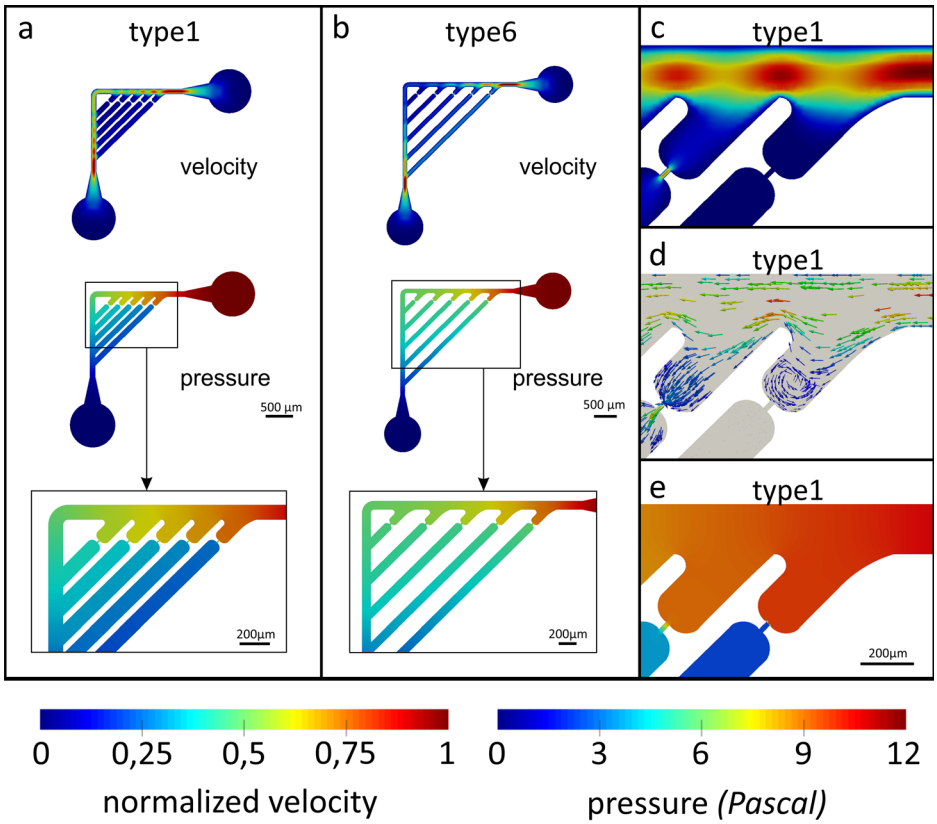

FIG. 4. Computational Fluid Dynamics (CFD) for channel types 1 and 6. (a), (b) Trap types 1 and 6 colored by contours of the velocity magnitude (top) and pressure field (middle). The middle section of the pressure field is magnified (bottom). (c)–(e) Channel type 1 with an artificially blocked first trap. (c) Contours of velocity magnitude, (d) velocity vectors colored by velocity magnitude, (e) Contours of pressure field. The velocity field is made dimensionless by the maximum flow velocity (normalized velocity) and the pressure is given in *Pascal*.

types 1 and 5 are equipped with 10 μm trap gaps each and types 2 and 6 with 20 μm trap gaps, respectively. As Table II shows, the flow ratios are slightly different between channel types 1 and 5 compared to channel types 2 and 6. This is caused by the altered inter-trap distance and the altered path length of the main channel, which slightly increases the resistance of the main channel path. This circumstance caused a 7% to 10% lower fluid volume passing the main channel in types 5 and 6 in comparison to channel types 1 and 2. Figures 4(c) and 4(d) show the flow rate situation, if trap 1 in channel type 1 was blocked. It can be observed that in this case the pressure loss is increased by less than 1 Pa. The pressure loss at a defined position along the path directly correlates with the acceleration of the fluid and therefore the shear stress

TABLE II. Mass flow rate proportions at the different traps and the pressure gradient in different channel types being in the open state and in channel type 1 in the case of an artificial blockade of the first trap.

	Unit	Type 1	Type 2	Type 5	Type 6	Type 1, trap 1 blocked
Trap 1	%	10.52	22.78	15.46	28.02	0.00
Trap 2	%	8.9	18	12.2	20.96	9.94
Trap 3	%	7.06	13.75	9.08	17.83	7.9
Trap 4	%	5.43	10.4	6.13	10.21	6.07
Trap 5	%	3.8	7.75	3.27	5.59	4.25
Main path	%	64.29	27.32	53.87	20.38	71.84
Pressure gradient	Pa	11.88	9.24	15.86	11.78	12.66

the particles are exposed to. As the drop of pressure from the first to the last trap varies in the range of only a few Pascal, the pressure conditions in the single traps were more or less well balanced and, moreover, ranged at relatively sensitive values. The results of the numerical simulations can be summarized as follows. (i) The triangle shape of this microfluidic structure shows a small total pressure loss, which is about one order of magnitude smaller compared to the meandering type structures. (ii) For a constant flow rate, the meander-structure shows a drastic change of the overall pressure level in the system if traps are blocked by beads or cells (or unblocked by cells which are squeezed out, more details are given in the Discussion section). Abruptly, the flow has to take a longer path through the meander-structure (or can take a shorter path through the unblocked trap). The smooth change of the total pressure level in blocked or unblocked trap situations is an inherent advantageous property of the triangle shape structure.

B. Trapping results

All types of cell trap devices investigated were highly effective in capturing beads (Fig. 5) of different diameters (30, 60, 80 μm) and snail neurons of varying size (20–100 μm) (Figs. 7 and 8). The only exception was the combination of channel type 1 with large 80 μm beads. No differences could be found in the trapping efficiency that depended on flow velocity. The order of occupancy generally did not follow the order of traps. In most cases, a more or less random occupancy of traps occurred.

1. Beads

Based on the simulation analysis of the microfluidic channel system, the trapping efficiency of the system was estimated quantitatively in experiments with beads (Fig. 6). As mentioned in the Materials and Methods section, efficiency was defined by taking three different criteria into account: 1. The general success of an experiment. 2. The particle loss. 3. The extent of multi-trapping. A comparison of the four different channel types shows that all channel types were highly reliable in successfully capturing particles of all tested sizes, except one situation, i.e., the combination of channel type 1 and large beads of 80 μm diameter succeeded in only 50% of all trials according to the criteria mentioned above. In all other combinations of bead size and channel type, between 80% and 100% of the experiments led to a positive outcome. The

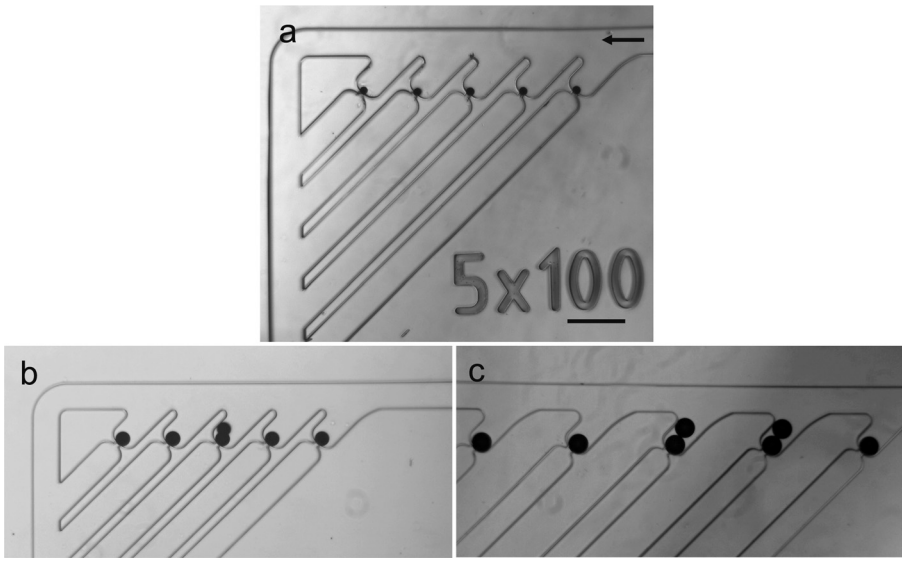

FIG. 5. Phase contrast images of trapping results with polystyrene beads of 30 μm (a), 60 μm (b), and 80 μm (c) in microfluidic trapping devices of type 1 (a), type 2 (b), and type 6 (c). In (b) and (c), some traps are occupied by two beads each and the remaining traps contain one single bead each. The arrow in (a) indicates the flow direction. Scale bar: 200 μm.

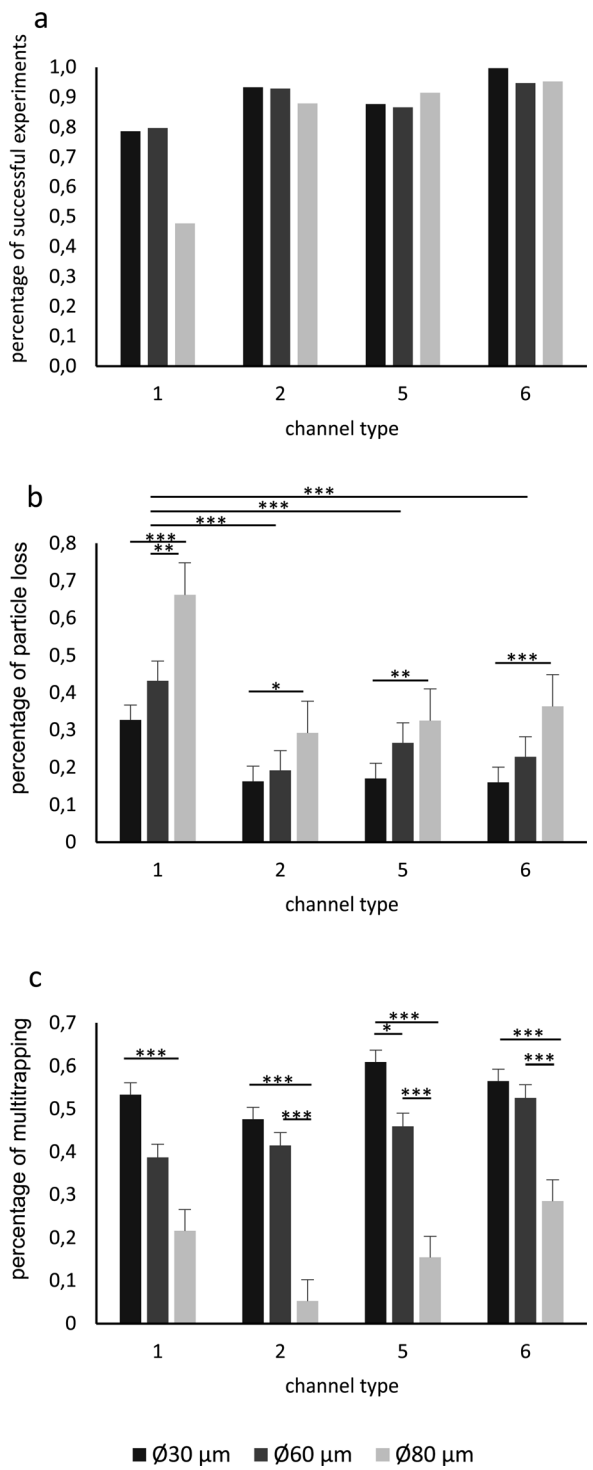

FIG. 6. Trapping conditions in microfluidic channels in dependence of channel type and particle size. (a) Overall trapping success. (b) Trapping efficiency as a function of particle loss. (c) Ratio of multitrapping. *, **, *** indicate significant differences estimated by post hoc Tukey test. * = $p < 0.1$; ** = $p < 0.05$; *** = $p < 0.01$.

results concerning particle loss showed that independent of the channel type, a deflection of beads towards the traps worked best with small beads of 30 μm, almost equally well with 60 μm beads which slightly tends to the worst case using 80 μm beads [Fig. 6(b)]. Particle loss in channel types 2, 5, and 6 showed no significant difference. On average, in these channel

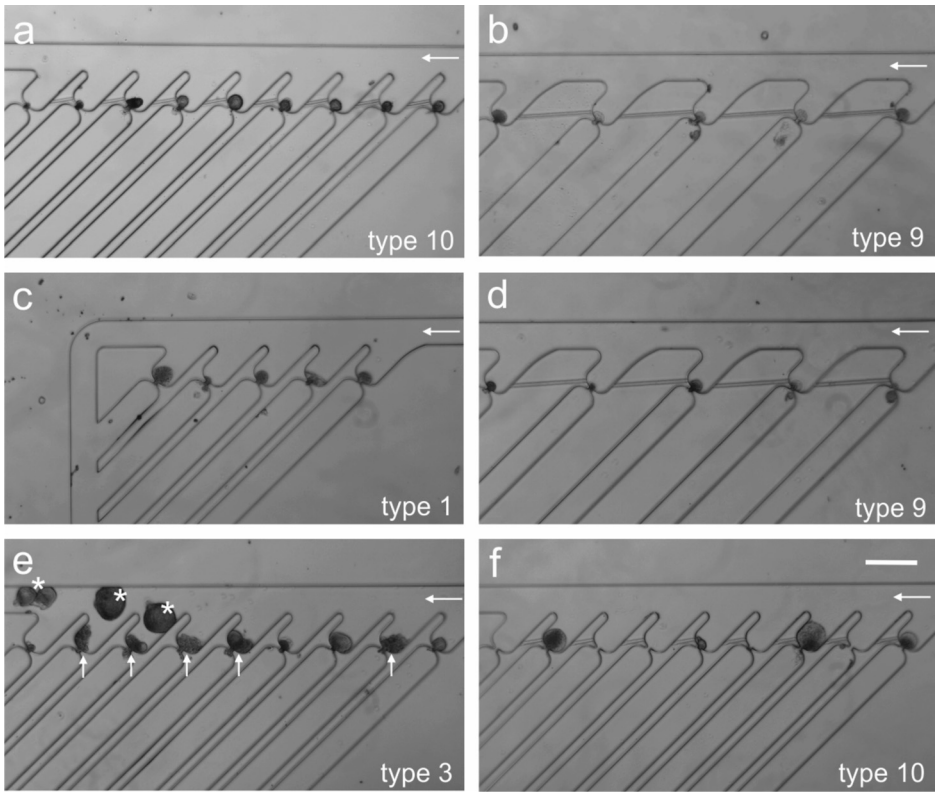

FIG. 7. Phase contrast images of trapping results with pond snail neurons in different cell trap devices. (a)–(f) Neurons of different diameters occupying the cell traps. (e) Vertical arrows at trap 2, 5, 6, 7, and 8 show filled traps by additional non-neuronal tissue. Horizontal arrows indicate the flow direction. Asterisks mark late arrived large neurons that were not deflected as already captured particles reduced the deflection force. Scale bar: 200 μm.

systems, particle loss of only 15% was observed with small beads, using 60 μm beads it ranged between 20% and 25%. Particle loss of 80 μm beads ranged between nearly 30% and about 35%. These values differed significantly from those obtained for smaller beads. The experiments with channel type 1 showed higher particle loss. With about 75% in average, particle loss was exceptionally large in channels of type 1 when using 80 μm beads. Multitrapping events occurred independently from the channel type and more with beads of small and

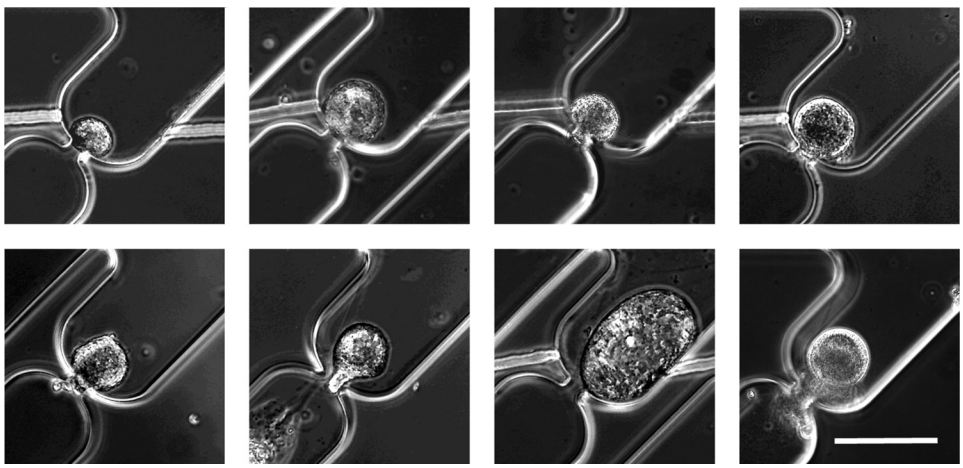

FIG. 8. Phase contrast images of captured pond snail neurons of different sizes appearing in a viable condition. Scale bar: 100 μm.

medium size, i.e., in about 40% to 60% of all cases. Multitrapping for 80 μm particles was limited to a maximum value of about 30% [Fig. 6(c)].

2. Cells

Molluscan neurons from *Lymnaea stagnalis* of diameters between 20 and 100 μm could be captured reliably with all presented channel types at low flow rates of 1 μl·min^{-1}. A selection of trapping results is shown in Fig. 7.

Deflection towards the transverse channels was increased in devices with trap gap widths of 20 μm than in those with 10 μm. This corresponds well to the results of the simulation described above. However, in devices with wider trap gaps, cells could not be captured as reliably as it was possible with smaller trap gaps. Some neurons were squeezed through the larger gaps. Therefore, devices with trap gaps of 10 μm width were more efficient in maintaining the viability of the captured cells. With the exception of the influence of the trap gap width, results were similar between different device types. Impurities in the cell suspensions occasionally resulted in traps becoming occupied by non-neuronal tissue [vertical arrows, Fig. 7(e)]. Neurons arriving later eventually did not find a free trap any more, where the deflection force was strong enough [asterisks, Fig. 7(e)]. The viability of trapped cells generally was not influenced by the trapping procedure, as the color and the shape appeared viable after the procedure (Fig. 8). Neurons inside the trapping areas survived for up to 7 days.

IV. DISCUSSION

A completely new designed channel device was used to apply the characteristics of continuous flow microfluidics to guide and position neurons of the pond snail *Lymnaea stagnalis*. Successful cell trapping in microfluidic systems with a meander shaped geometry was reported in the literature for cell suspensions of different types, such as yeast cells,[27] cancer cells,[24] and stem cells.[25,29] However, it turned out that these common designs with meandering channels were not functional with invertebrate neurons. The concept of common meander-shaped channel geometries for cell trapping is based on a differential fluidic resistance of two streams. The design enables the serial arraying of cells in trapping areas along the stream of less resistance, acting as a valve in the open state.[28] In contrast, the triangle shaped microfluidic channel system presented here offers a simple geometrical design with more balanced flow ratios and with a parallel rather than a serial connection of the separate pathways. Simulation experiments were performed to compare the serpentine structures with the new triangle design in order to try to explain the different properties and therefore suitability of the systems for sensitive cells such as pond snail neurons. The analysis showed crucial differences in the pressure profiles (supplementary material: Fig. 1; Tables III and IV) and therefore give information about the disadvantages of the meandering structure for sensitive cells. The pressure profile in meandering structures showed values which are about 30 times higher than in the triangle design and causes a fast drop of pressure from the first to the last trap along the short path through the trapping areas [supplementary material: Figs. 1(c) and 1(d)]. Thus, this large total fluidic resistance of the meandering system impedes loading of large cells at low flow velocities. Furthermore, the trapped cells are exposed to high mechanical stresses due to the large pressure level [supplementary material: Fig. 1(e); Table IV). In fact, the meandering design enables a high trapping efficiency as the fluidic pressure difference is the main driving force for the cell into the trap. However, too fast pressure changes increase the fluidic shear stress on a trapped cell at the same time. As a result, it seems that cell types that were successfully applied with the meandering type[24,25,27] have to be very robust and rigid because negative influences on cell viability were only rarely discussed in earlier applications.[30]

Neurons, maybe not only from invertebrates, are sensitive, especially regarding fluidic pressure and shear stress at high flow velocities. Neurons, the larger they are, deform easy, which increases the risk of membrane damages in trapping conditions. As a consequence, in our experiments, *Lymnaea* neurons squeezed through the narrow trap gaps of microfluidic channel devices from the meandering type due to their high deformability (data not shown). To make

use of the advantages of invertebrate neurons in network research on MEAs,[3] it was therefore necessary to develop an alternative channel design that conforms to the requirements of these neurons.

The triangle shaped microfluidic channel system presented here for the first time offered adequate pressure conditions for invertebrate neurons. It is most likely that also other pressure and shear-stress sensitive cell types can be processed more successfully with this new triangle shaped structure. In spite of a small flow rate through the trapping areas, the system provided a reliable trapping efficiency, which was comparable to the results shown with meandering channel structures.[25] Due to the simple channel geometry, without long paths, many curves and edges, the overall fluidic resistance was kept to a minimum, which facilitated particle loading at low flow rates, which was a problem with the meandering channel type and large volume pond snail neurons (data not shown). Furthermore, due to the parallel and not serial connection of the separate pathways, the fluidic pressure was more balanced, which did not affect the trapping efficiency. The drop of pressure was significantly reduced, which essentially decreased the mechanical stress for trapped cells in the trapping areas. For the same reasons, the system was far less prone to disturbances evoked by temporal blockings of single channel parts. Because of these facts, the new triangle system may turn out to be applicable more universally for many different cell types.

Simulation of the flow proportions in a channel system could deliver important information of the general suitability of a system, but it was unable to predict the actual behavior of inserted particles with certainty. The triangle system was designed with different parameter variations to test for the one best suitable for practical use. Trapping efficiency that directly correlated with the percentage of particle loss was tested in four different channel types differing mainly in the trap gap width and inter-trap distance. It can be concluded that the deflection force necessary to guide particles into the traps mainly depended on the resistance of the transverse channels, which was strongly influenced by the trap gap width. As the simulation showed, the mass flow rate through the transverse channels in 20 μm trap gap types was about twice as large as for the smaller trap gap types. Fitting to the theoretical results, least trapping efficiency tested with beads was observed in channel type 1 with a trap gap width of 10 μm, while the other tested designs showed similar efficiencies on a high level. This was even true for channel type 5 having a small trap gap width as well. These results let us assume that not only the fluidic resistance determined by the trap gap width influenced the trapping efficiency but also the inter-trap distance must have a perceptible effect. Therefore, the larger distance of 400 μm in type 5 channels seemed to be able to compensate the narrow trap gap. Probably, cells in channels with larger distances between the single trapping areas had more time to change their orientation. Therefore, they might be able to change between different stream lines, which might influence the actual deflection towards the traps decisively.

In the past, a channel dimension about 30% to 40% higher than the largest cell diameter was predicted to work best regarding cell guiding and the avoidance of channel blocking.[25] However, contrary to this assumption, experiments with 30 μm beads in 100 μm channels showed the lowest particle loss consistently. This observation is confirmed by the concept of hydrodynamic filtration introduced by Yamada and Seki.[37] They showed an efficient particle trapping in different channel designs with a channel width clearly larger than the particle size. Yamada and Seki[37] but also Occhetta and colleagues[38] showed a flow rate-dependent size limit of particles, which have to be trapped. The flow rate entering the transverse channels and the corresponding "virtual width" of the flow determines the deflected particle size and is itself determined by the microchannel dimensions. It is suggested that the particles follow the flow line that passes the center of its mass. Consequentially, the flow width entering the transverse channel is required to be at least as wide as the particle's own radius. From this, it follows that in a given trapping system, smaller particles can be trapped more easily than larger particles, which is in agreement with the findings of this study. Consequently, a change in microchannel dimension with increased channel width and probably height should increase the deflection rate of larger (80 μm) beads. But, unlike the descriptions in the literature, the trapping of larger particles is not excluded by the given channel geometries and the accompanied distribution of flow

in this study. However, a certain degree of particle loss was observed because particles in the main channel moving (or following streamlines) close to the opposite side of the transverse channels were not deflected towards the cell traps. Although the location of the individual cell in the main channel seemed to be more or less random, it was possible to achieve extraordinary good trapping performance with small beads and cells. This fact let assume that particles may not inevitably follow their streamlines but are able to change between them, especially deformable and such as snail neurons.[37]

Trapping efficiency was much better than the results from the simulation predicted. Previously, the necessity of a flow ratio of 1:2 to 1:3 for a reliable trapping efficiency was postulated.[25,28] Even though these conditions were not satisfied with the triangle geometry, we recorded only small cell loss percentages. In general, the insertion of, on average, twice as much beads/neurons was sufficient to fill all traps of a channel system, which corresponds to results of Kobel and colleagues[25] who needed about 1000 cells to fill 400 traps. In many experiments with beads but also with cells, and independent from the channel type, multitrapping was observed. Multitrapping is described as a common problem.[23,25,39,40] The extent of multitrapping is strongly dependent on the bead size. Thereby, multiple trap occupancy occurred more often with 30 μm beads as with 60 and 80 μm beads, which can be explained by the trap gap dimension. Larger beads were able to block the trap gap almost completely, in contrast to the small beads of 30 μm diameter. A decreased height of the trapping area compared to the main channel would improve the channel block of the trap gap by a trapped cell and reduce multitrapping events.[25] However, from our experience, we would expect a reduced trapping efficiency by decreasing the trap gap height because of an increase in the flow resistance. The simulation results showed remaining flow into the trapping areas even if the trap gap is blocked entirely [Fig. 4(d)]. Thus, the avoidance of multitrapping events seems to be nearly impossible, unless the trap size would always perfectly fit the cell size, so that it leaves no room for a second cell. For cell populations with a high heterogeneity in size, the implementation of suitable trap dimensions in the context of a guaranteed single cell trapping will be a challenge for the future.

Experiments with beads turned out to be a helpful tool to characterize flow dynamics and particle behavior inside the new channel design quantitatively. However, as artificial beads are immune to inadequate pressure conditions and shear stress, positive results from bead experiments were not sufficient to be transferred to the biological test system. Therefore, the triangle systems were also tested with *Lymnaea* cell suspensions. In contrast to the experiments with serpentine channels, here, invertebrate neurons could be successfully trapped and maintained in a viable state.

Finally, the comparison of the serpentine channel system with the new triangle design taught us that the individual needs of a certain cell system may force channel designers to make compromises between theory and praxis. However, as we are interested in the investigation of really small networks *in vitro*, a neuron population of 3 to 10 represents an optimal condition regarding our approach. However, our results from simulation let us conclude that the number of traps does not affect the functionality and can be extended as needed. Furthermore, we are developing ideas to expand the number of traps in a space-saving manner. Both approaches should allow for a broader application of the system shown here. Anyway, the exceedingly satisfying results, which could be achieved, pushed us a crucial step forward towards a universal solution for the positioning problem of cells *in vitro*.

V. CONCLUSION

A complete new microfluidic channel design for a sensitive and efficient trapping of invertebrate neurons is presented. Geometrical improvements compared to the serpentine type, resulting in a triangle shaped device, decreased the overall pressure gradient and balanced pressure conditions on individual trapping areas but maintained functionality in terms of trapping efficiency at the same time. Within this study, the characterization of the functionality of 4 out of 10 different geometrical variants with polystyrene beads of different sizes to find most suitable

parameter combinations in terms of particle size, trap gap width, and inter-trap distance was shown. Concerning the trapping efficiency and minimal possible multitrapping events, the best fitting parameter combinations met each other in channel type 6 and medium large particles of 60 μm. Positive results could be achieved with all 10 channel types by applying invertebrate neurons. However, as qualitative observations with cells revealed improved trapping results, in the context of maintained viability, by using smaller trap gaps, channel type 5 or 7 for future applications with pond snail neurons would be recommended. Next steps towards an integrated biohybrid system for basic physiological cell analysis could be a further optimization of geometrical parameters and an integration of electrodes into the trapping areas.

SUPPLEMENTARY MATERIAL

See supplementary material for further CFD results revealing pressure conditions and flow rates for several trap configurations of the triangle channel design and of a common used serpentine system.

ACKNOWLEDGMENTS

We thank Akram el Hasni from the Institute of Materials in Electrical Engineering 1, RWTH Aachen University, for his assistance in photolithography.

[1]A. Minerbi, R. Kahana, L. Goldfeld, M. Kaufman, S. Marom, and N. E. Ziv, PLoS Biol. **7**, e1000136 (2009).
[2]D. Kleinfeld, F. Raccuia-Behling, and H. J. Chiel, Biophys. J. **57**, 697 (1990).
[3]P. Massobrio, C. N. G. Giachello, M. Ghirardi, and S. Martinoia, BMC Neurosci. **14**(1), 22 (2013).
[4]C. A. Thomas, P. A. Springer, G. E. Loeb, Y. Berwald-Netter, and L. M. Okun, Exp. Cell Res. **74**, 61 (1972).
[5]J. L. Novak and B. C. Wheeler, J. Neurosci. Methods **23**, 149 (1988).
[6]G. W. Gross, B. K. Rhoades, H. M. Azzazy, and M. C. Wu, Biosens. Bioelectron. **10**, 553 (1995).
[7]D. A. Wagenaar and S. M. Potter, J. Neural Eng. **1**, 39 (2004).
[8]B. Eversmann, M. Jenkner, F. Hofmann, C. Paulus, R. Brederlow, B. Holzapfl, P. Fromherz, M. Merz, M. Brenner, M. Schreiter, R. Gabl, K. Plehnert, M. Steinhauser, G. Eckstein, D. Schmitt-Landsiedel, and R. Thewes, IEEE J. Solid-State Circuits **38**, 2306 (2003).
[9]M. Ballini, J. Müller, P. Livi, Y. Chen, U. Frey, A. Stettler, A. Shadmani, V. Viswam, I. L. Jones, D. Jäckel, M. Radivojevic, M. K. Lewandowska, W. Gong, M. Fiscella, D. J. Bakkum, F. Heer, and A. Hierlemann, IEEE J. Solid-State Circuits **49**, 2705 (2014).
[10]J. R. Buitenweg, W. L. Rutten, W. P. Willems, and J. W. van Nieuwkasteele, Med. Biol. Eng. Comput. **36**, 630 (1998).
[11]K. Göbbels, A. L. Thiebes, A. van Ooyen, U. Schnakenberg, and P. Bräunig, J. Insect Physiol. **56**, 1003 (2010).
[12]M. Suzuki, K. Ikeda, M. Yamaguchi, S. N. Kudoh, K. Yokoyama, R. Satoh, D. Ito, M. Nagayama, T. Uchida, and K. Gohara, Biomaterials **34**, 5210 (2013).
[13]M. Merz and P. Fromherz, Adv. Mater. **14**, 141 (2002).
[14]E. Claverol-Tinturé, M. Ghirardi, F. Fiumara, X. Rosell, and J. Cabestany, J. Neural Eng. **2**, L1 (2005).
[15]J. Erickson, A. Tooker, Y.-C. Tai, and J. Pine, J. Neurosci. Methods **175**, 1 (2008).
[16]A. Takeuchi, S. Nakafutami, H. Tani, M. Mori, and Y. Takayama, Lab Chip **11**, 2268 (2011).
[17]K. Krumpholz, J. Rogal, A. El Hasni, U. Schnakenberg, P. Bräunig, and K. Bui-Göbbels, ACS Appl. Mater. Interfaces **7**, 18769 (2015).
[18]A. M. Taylor, S. W. Rhee, C. H. Tu, D. H. Cribbs, C. W. Cotman, and N. L. Jeon, Langmuir **19**, 1551 (2003).
[19]S. W. Rhee, A. M. Taylor, C. H. Tu, D. H. Cribbs, C. W. Cotman, and N. L. Jeon, Lab Chip **5**, 102 (2005).
[20]A. M. Taylor and N. L. Jeon, Curr. Opin. Neurobiol. **20**, 640 (2010).
[21]M. Mehling and S. Tay, "Microfluidic cell culture," Curr. Opin. Biotechnol. **25**, 95 (2014).
[22]J. W. Park, H. J. Kim, M. W. Kang, and N. L. Jeon, Lab Chip **13**, 509 (2013).
[23]D. Di Carlo, L. Y. Wu, and L. P. Lee, Lab Chip **6**, 1445 (2006).
[24]J.-P. Frimat, M. Becker, Y.-Y. Chiang, U. Marggraf, D. Janasek, J. G. Hengstler, J. Franzke, and J. West, Lab Chip **11**, 231 (2011).
[25]S. Kobel, A. Valero, J. Latt, P. Renaud, and M. Lutolf, Lab Chip **10**, 857 (2010).
[26]Y. Takayama, N. Kotake, T. Haga, T. Suzuki, and K. Mabuchi, J. Biosci. Bioeng. **114**, 92 (2012).
[27]L. Bell, A. Seshia, D. Lando, E. Laue, M. Palayret, S. F. Lee, and D. Klenerman, Sens. Actuators, B **192**, 36 (2014).
[28]W.-H. Tan and S. Takeuchi, Proc. Natl. Acad. Sci. U.S.A. **104**, 1146 (2007).
[29]S. Kobel, O. Burri, A. Griffa, M. Girotra, A. Seitz, and M. P. Lutolf, Lab Chip **12**, 2843 (2012).
[30]N.-D. Dinh, Y.-Y. Chiang, H. Hardelauf, J. Baumann, E. Jackson, S. Waide, J. Sisnaiske, J.-P. Frimat, C. van Thriel, D. Janasek, J.-M. Peyrin, and J. West, Lab Chip **13**, 1402 (2013).
[31]H. G. Weller, G. Tabor, H. Jasak, and C. Fureby, Comput. Phys. **12**, 620 (1998).
[32]H. Jasak and H. G. Weller, Int. J. Numer. Methods Eng. **48**, 267 (2000).
[33]P. Renze, A. Buffo, D. L. Marchisio, and M. Vanni, Chem. Ing. Tech. **6**, 1088 (2014).
[34]G. Kemenes and P. R. Benjamin, Curr. Biol. **19**, R9 (2001).
[35]R. L. Ridgway, N. Syed, K. Lukowiak, and A. G. M. Bulloch, J. Neurobiol. **22**, 377 (1991).

[36]R. K. Kaul, Ph.D. thesis, Technical University Munich, Munich, 2007.
[37]M. Yamada and M. Seki, Lab Chip **5**, 1233 (2005).
[38]P. Occhetta, M. Licini, A. Redaelli, and M. Rasponi, Med. Eng. Phys. **38**, 33 (2016).
[39]S. Faley, K. Seale, J. Hughey, D. K. Schaffer, S. VanCompernolle, B. McKinney, F. Baudenbacher, D. Unutmaz, and J. P. Wikswo, Lab Chip **8**, 1700 (2008).
[40]S. H. Jin, S. Jang, B. Lee, H. Jeong, S. Jeong, S. S. Lee, K. P. Kim, and C. Lee, Lab Chip **16**, 1358 (2016).